***Research Article***

Chemical Review and Letters
journal homepage: www.chemrevlett.com
ISSN (online): 2645-4947 (print) 2676-7279

# Electronic and optical properties of 2D VFeSb: case study by DFT

Morug Salih Mahdi[1], Hiba Mushtaq[2], Dheyaa Flayih Hasan[3], Hala Bahair[4], Ameer Hassan Idan[5], Farnaz Behmagham[6, *]

[1]*College of MLT, Ahl Al Bayt University*
[2]*Gilgamesh Ahliya University, Baghdad, Iraq*
[3]*College of Health and Medical Technology, National University of Science and Technology, Dhi Qar, 64001, Iraq*
[4]*Medical technical college, Al-Farahidi University, Iraq*
[5]*Al-Zahrawi University College, Karbala, Iraq*
[6]*Department of Chemistry, Islamic Azad University, Miandoab, Iran*

ARTICLE INFO

*Article history:*
Received 05 May 2024
Received in revised form 22 June 2024
Accepted 24 June 2024
Available online 08 July 2024

*Keywords:*
half metals,
heusler,
monolayer,
optical,
band structure.

ABSTRACT

We propose the two-dimensional (2D) structure of VFeSb and investigate their structural, electronic and optical properties in the framework of first-principles calculations and density functional theory (DFT). By calculating the E-V curve, we found that VFeSb has mechanical stability. From the electronic point of view, this structure is a half metal, which has the integer magnetic moment, so it is a suitable candidate for use in spintronics applications. The dielectric function curve showed that the greatest response to the incident photon and electron transition occurs in the IR and visible light regions, which is suitable for use in optoelectronics. The refraction and extinction coefficients show that in the IR and visible light regions, the amplitude of electromagnetic waves is low, and the reflection coefficient is less than 40% in most energy regions and the V structure behaves transparently.

## 1. Introduction

Half metallic properties in materials have always attracted the attention of scientists. These materials are conductive in the majority spin and semiconducting in the minority spin. Semimetals are divided into two main categories: binary compounds [1-4] and Heusler compounds. The structure of Heuslers are divided into two categories: full Heuslers and half Heuslers [5-9]. Half Heusler such as VFeSb [10] compounds with XYZ Stoichiometry play an important role in the spintronics industry. In these compounds, X and Y atoms often belong to TMDs and Z atoms belong to groups III to V of the periodic table. One of the most important features of Heuslers is their crystallization at room temperature and their crystalline strength. These compounds have been used many times as thin films and heterojunctions in the spintronics industry [11-13].

Heusler films are often grown in (001) and (111) directions according to their selected substrates [14, 15]. Considering that these compounds are based on the fcc crystal structure and space group$F\bar{4}3m$, so their top surface is hexagonal in the (111) direction, and one of the reasons for the hardness of the crystal in Heusler compounds is the existence of this tight-packed structure. In recent years, in addition to the experimental growth of Heusler thin film films in (111) direction have introduced it with a thickness of several atoms in the majority of a graphene-like geometry [16, 18]. In recent years, in addition to the experimental growth of Heusler thin film films along the (111) direction, the two-dimensional graphene-like structure of these compounds has also been discussed and investigated, and a multilayer structure of its (111) film have been introduced with a thickness of several atoms in the majority of a graphene-like geometry [19].

The half Heusler VFeSb, which has been experimentally sputtered at room temperature in recent years [20], has been the subject of our attention in this work. This compound in the bulk state has a metallic

* Corresponding author; e-mail: behmagham_farnaz@yahoo.com
https://doi.org/10.22034/crl.2024.455831.1333

characteristic with a total magnetic moment of 3.2 $\mu_B$ and has a relatively high crystal hardness, which is about 1.5 times that of steel metal. In recent years, most of the work has focused on the electronic and mechanical properties of VFeSb bulk. Therefore, we chose the two-dimensional hexagonal structure of this half metal to investigate its structural, electronic and optical properties, so that we have studied and analyzed these results in the next parts of the article.

## 2. Computational method

In this work, the physical properties of the two-dimensional VFeSb half-metal compound were studied by first-principle calculations based on the density functional theory (DFT) [21] and considering the generalized gradient approximation of GGA [22,23] in order to calculate the exchange-correlation potential and also to measure the energy gap. Spin-polarized calculations were done using wien2k code [24, 25]. In order to calculate the cut-off parameter RK_max = 7, the number of k_points in the first Brillion zone was chosen to be 500 points, which was reduced to 50 points in the inverse space due to the symmetry of the crystal and the selection of the appropriate space group No.156. We have taken the radii of Moffin-Tin spheres of Fe, V and Sb atoms as 2.3, 2.1 and 1.9, respectively. Moreover, the run scf calculation accuracy is selected to 0.00001 on electronic charge, and also, the optical calculations have been done by RPA approximation [26].

## 3. Results and Discussion

### 3.1. Structural properties

Considering that the half Heusler structure of VFeSb has been synthesized in the bulk phase before, this gives us more hope that in the future we will be able to witness the synthesis of a single layer of this compound in (111) direction. Figure 1(a,b) shows the unit cell of the two-dimensional structure of VFeSb in top and side views. This graphene-like structure of CoVSb occurred from cutting the bulk structure of this compound in the FCC phase and along the (111) direction. As we can see from the top view in Figure 1a, the two-dimensional structure of VFeSb has a hexagonal structure. Of course, according to Figure 1b, it can be seen that this structure includes three atomic layers of V, Fe and Sb, so that the V atom is placed exactly below the Fe atom. Considering that V and Fe atoms are located in the upper and lower levels of this monolayer structure and both of these atoms have half-filled d orbitals, therefore, we see the presence of free electrons in the upper and lower levels, which causes a change in the physical nature of this structure.

The first step in examining the physical characteristics of this structure is to examine its mechanical stability. For this purpose, the curve of changes of the total energy of the unit cell of this composition has been examined in the c/a ratio (E-V), which is shown in Figure 1c. We can see, this curve has a Minimum point, which represents the equilibrium volume and the ground state point for this structure. The hidden point in this figure is that the slope of the curve on the right side of the minimum point is steeper than on the left side, which shows that more pressure is needed to create strain than for stress. On the other hand, the steep slope of the curve indicates the high hardness of the VFeSb structure.

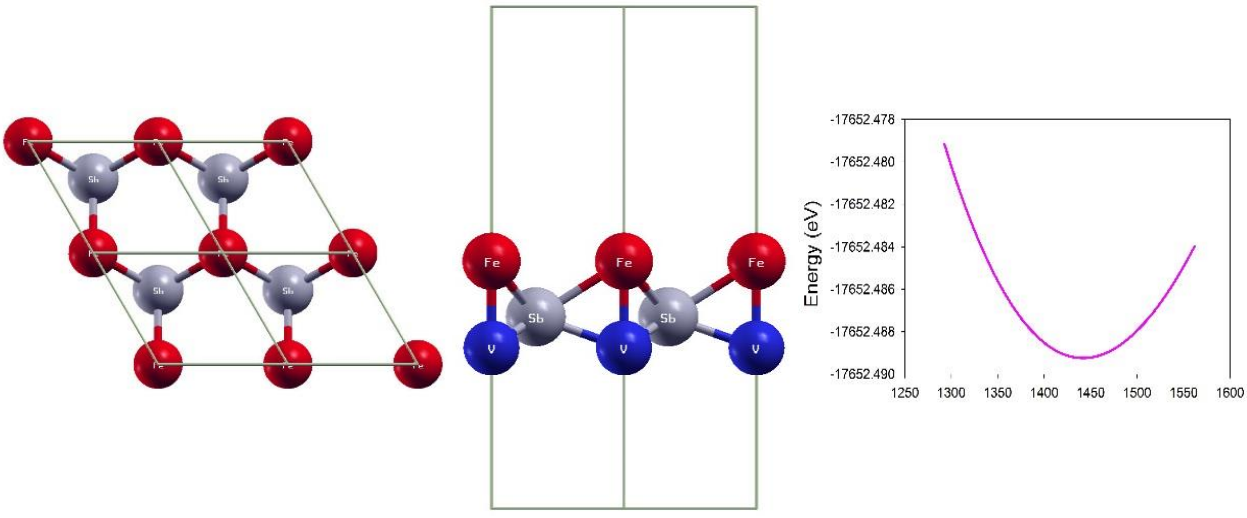


**Fig. 1.** Geometrical structure of 2D VFeSb in top and side view, also (c) E-V curve of this structure.

### 3.2. Electronic properties

The most useful tools for detecting the electronic properties of materials are the density of state (DOS) and the band structure curves through which we examine the electronic properties in this paper. Figure 2a shows the DOS diagram of the 2D structure of VFeSb in up and down spins for better comparison. It can be seen that we see strong magnetic anisotropy in the Fermi level. As we see metallic behavior in spin up and semiconducting behavior in spin down, so this composition is a half metal with 100% spin polarization. The total magnetic moment of this combination is an integer of5.0 $\mu_B$, which is considered a large magnetic moment for semi-metals. In spin down, the structure is an n-type semiconductor with an electron gap of about 0.7 eV. The sawtooth shape of the curves is due to the presence of free electrons on the surface of this 2D structure. Another point is that in the conduction region in both spins, we see the continuity of the DOS diagram, so excited electrons due to heat or potential difference flow well in this region.

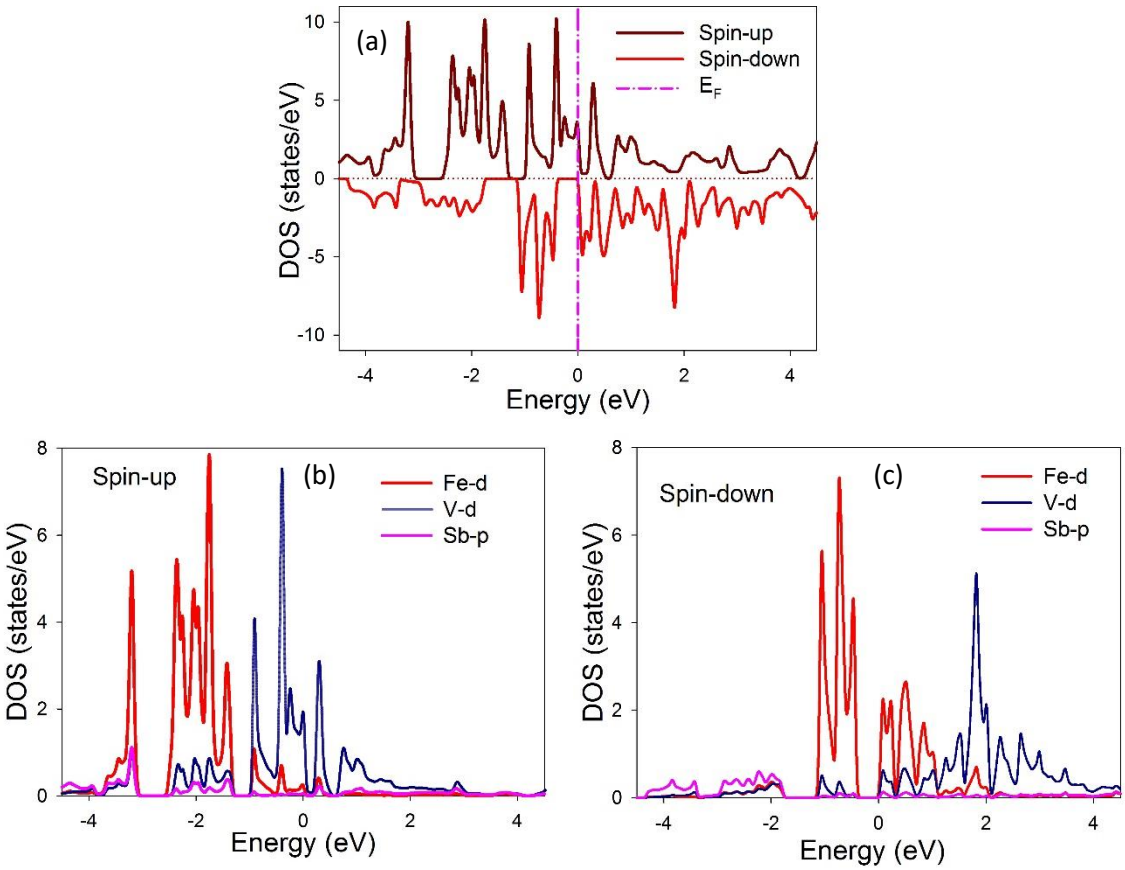


**Fig. 2.** (a)Total DOS (b, c) p-DOS of effective orbitals in the structure for up and down spins.

In order to further investigate the electronic properties and the type of bonds, we have shown the DOS diagram of the effective orbitals of all three Fe, V and Sb atoms in Figure 2(b, c). we can see that the highest contribution of electrons in Fe and V atoms belongs to d orbitals and in Sb atom is related to p orbital of this atom and also the overlap of d orbitals of two Fe and V atoms and p orbital of Sb atom is indicative of d-d and p-d bonds between This is atoms. In spin down, the main reason for the splitting of the DOS diagram in the energy gap region is the overlap of d orbitals of Fe and V atoms. In this spin, the largest contribution of electronic states and the electron injection source is d orbital of Fe atom. At energies higher than zero (conduction region), d orbitals of Fe atom in the range of 0-1.5 eV and d orbitals of V atom from 1.5 eV provide the highest contribution in creating conduction conditions. But in spin up, the metallic and conductive factor belongs entirely to the d orbitals of the V atom, which is separated from the Fermi range by a small gap in the energy region of 1.5 eV.

In figure 3a and 3b, the band structure of 2D VFeSb is drawn in the Γ-M-K-Γ symmetry path in up and down spins.

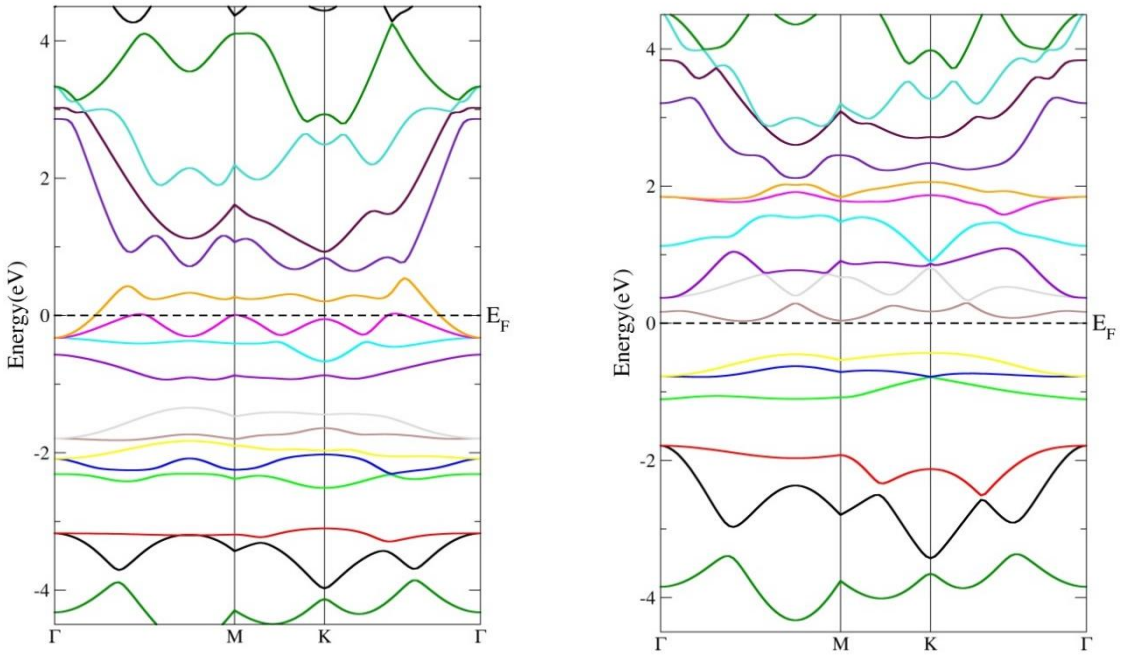


**Fig. 3.** Band structure for the 2D structure of VFeSb in up and down spins.

In the up spin and in the Γ-M and K-Γ directions, the Fermi level is crossed twice by an electron level that belongs to the d orbital of the V atom. But in the spin down, we see the splitting of the levels in the Fermi level, so that an indirect band gap of 0.7 eV appears in this interval. In spin down, the high density of levels on the sides of the Fermi surface and very suitable band gap, as well as the overlap and gradient of the levels in the conduction region, introduce this compound as a suitable candidate for thermoelectric and optical applications.

### 3.3. Optical properties

The most important optical parameter that shows the object's response to the light irradiated to it is the dielectric function [27, 28]. The dielectric function tensor consists of two real and imaginary parts. In Figure 4a, we have shown the real part (Re-ε(ω)) and in Figure 4b the imaginary part (Im-ε(ω)) in the x and z directions. The direction of the x-axis is for the case where the component of the electric field of the irradiated light is located in the 2D sheet of 2D VFeSb, and the direction of the z-axis is for the case where the component of the electric field of the light is perpendicular to the plane of the structure.

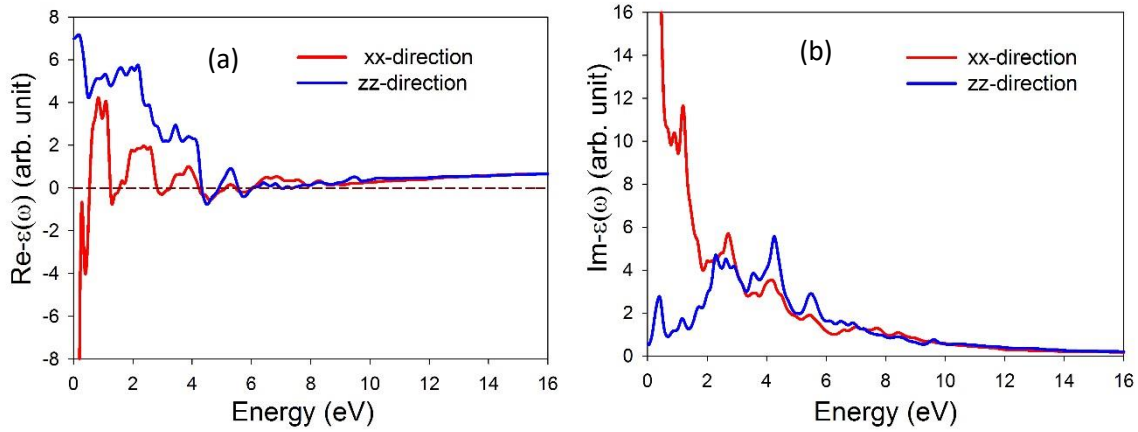


**Fig. 4.** (a) Real and (b) imaginary part of the dielectric function for the 2D VFeSb monolayer.

We can see that at low energies (infrared (IR), visible and UV edge) the material's response to the light emitted in the x and z directions is completely anisotropic. So that for the direction of the x-axis, the static value of Re-ε(ω) tends towards infinite values, but for the z-axis, it tends to the direction of +7 values, which indicates that the behavior of this object is completely metallic along the direction of the x-axis. And by applying light on this structure, the electrons are excited quickly and it shows a metallic behavior. With the increase in the energy of the radiated light in the IR region, we see a relatively long peak for the x direction, which we expect semi-conductivity due to its values. With the further increase of incident photon in this direction, this peak is repeated again with lower heights and eventually reaches a negligible value and less than 1 at energies higher than 5 eV, so that the value of ε is less than the vacuum, which indicates a completely clear behavior of this combination is along the x-axis. It should be mentioned that in the energy range of 0-6 eV along the x-axis, we see the emergence of 8 roots (Re (ω=0)), which can be indicative of plasmonic fluctuations. In the direction of the z axis, this behavior is repeated in a similar way, with the difference that its static value is 7 and the peaks formed in this direction are higher than in the x direction. Therefore, the response to the light emitted in the direction of the z axis is far greater than is in the x direction. Along the z-axis, we see 4 roots in the energy region of 4-6 eV, which is in agreement with the roots of the x-axis. The anisotropy of the optical response for the x and z directions makes it possible to get different responses from this combination by changing the direction of the irradiated light, and therefore we can use this combination as an optical switch.

Figure 4b shows the imaginary part of the dielectric function. It can be seen that in the IR region and the edge of the visible light, the x and z curves are completely asymmetric, but from the visible region onwards, it reaches a relative isotropy. Im-ε(ω) curve peaks represent intraband and interband transitions. It can be seen that the largest peaks of Im-ε(ω) in the IR region occurred in the x direction, so the main intraband transitions occur in the x direction. In the visible region, we see a decrease in the peak for the x direction, which represents three interband transitions for this direction. An interesting point is that the magnitude of the peaks at energies lower than the visible region belong to the x direction and higher than the visible region (e.g. 3 eV) belong to the z direction. Therefore, the effect of the lines in the electron transfer changes with the change of the direction of the irradiated light.

We have shown the curve of the energy loss function (Eloss) in Figure 5, that in the IR and visible regions, the magnitudes of the peaks are small for both directions, and with the increase of the radiated energy, the spectrum of the loss function increases and reaches a MAX value at 10 eV. This diagram shows that the VFeSb structure has the lowest amount of loss in the IR and visible regions. Therefore, the structure is a suitable option for use in optical instruments in the IR and visible region. The peaks of Eloss for both particles are in perfect agreement with the roots of Re-ε(ω), so it can be said that the plasmon frequency occurred along the x axis at energies of 3 and 4 eV and for the z direction at energies of 5 and 5.5 eV has occurred.

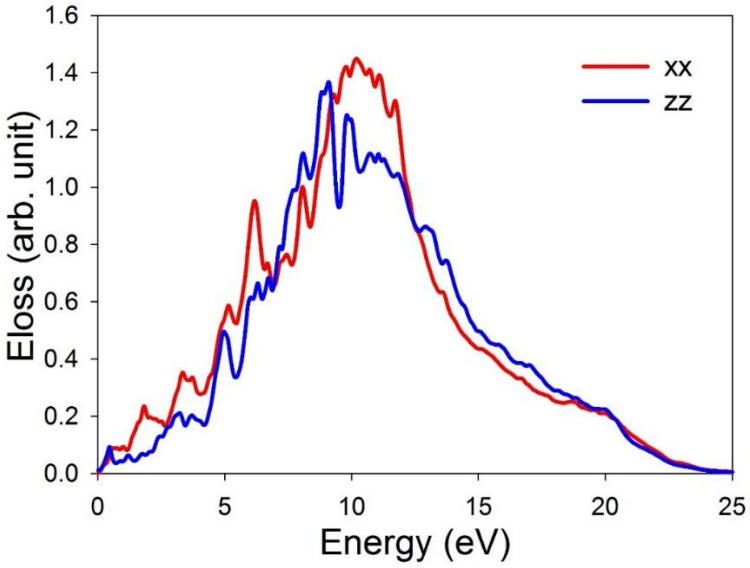


**Fig. 5.** Energy loss function (Eloos) for x and z symmetry directions.

In Figure 6a, we have drawn the refractive index (n(ω)) of the 2D structure of VFeSb in the x and z directions. The static value of the refractive index in the x direction is greater than 5 and in the z direction is about 2.7, which shows that in the x direction and at very low energies, this compound exhibits metallic behavior, but as soon as the incident photon energy increases, it suddenly disappears. It drops below the number 3, and after that, its value decreases with an oscillating downward slope, and it becomes less than 1 at energies higher than 5 eV.

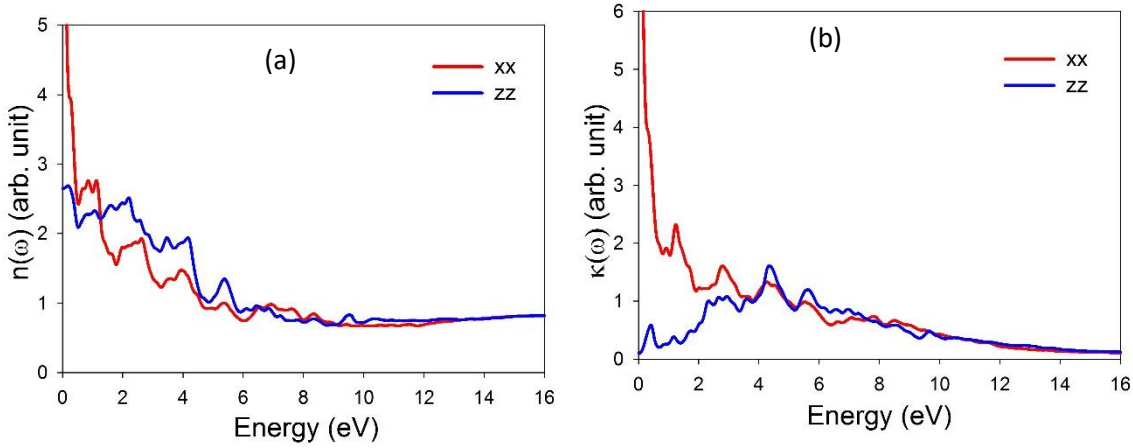


**Fig. 6.** (a) Refractive index and (b) extinction coefficient for the 2D VFeSb structure in x and z direction.

Similarly, we observe this behavior in the z direction. In the visible region and the UV edge, the values of n are larger than the values of n in the x direction, but the general behavior in both directions is completely similar in the visible region and beyond. The reduction of n in both directions to values less than 1 for energies greater than 5 eV shows that the superluminal phenomenon occurs in this compound and this compound exhibits transparent behavior at high energies.

Figure 6b shows the extinction coefficient for 2D VFeSb monolayer. We notice that in the x direction, like the refractive index of the static coefficient, the extinction coefficient is a very large number, and as soon as the energy of the irradiated photon increases, it decreases with a very steep slope. But in the visible area, the rate of descent is fluctuating and with a gentler slope. The behavior of the extinction coefficient along the x-axis and the refractive index at low energies shows that in the energy range of 0-1 eV we see optical stability in this direction. But in the z direction, the static value of the extinction coefficient is zero and up to 4 eV, it behaves opposite to the x direction, so it can be said that in the energy range of 0-4 eV, the extinction coefficient in the x direction is greater than in the z direction, so in the visible light region and IR light can better pass through this material in the z direction. Although the peaks of this curve are small in both directions, from 4 eV onwards, during an isotropic behavior, the extinction coefficient values show a decreasing behavior. In general, it can be said that in this structure, the amplitude loss of optical electromagnetic waves and loss in their amplitude is small, especially in the IR and visible region along the z-axis.

Figure 7 shows the reflection coefficient for this structure in the x and z directions. It can be seen that in the direction of x and in the IR region, in confirmation of other optical diagrams, we see optical instability for this direction. But in the direction of the z-axis, its static value is 0.2, which shows that most of the irradiated light passes through this object. Like other optical diagrams, these two diagrams are completely anisotropic at low energies, but they behave similarly from 4 eV onwards. Along the x-axis in the visible region, the values of the reflection coefficient are reduced in the form of an oscillating graph of apparent dip. Similar to this pulse behavior along the z-axis has occurred in the IR region and beyond. It can be seen that the amount of light reflection will always be less than 40%, so in both directions we see a transparent level for them.

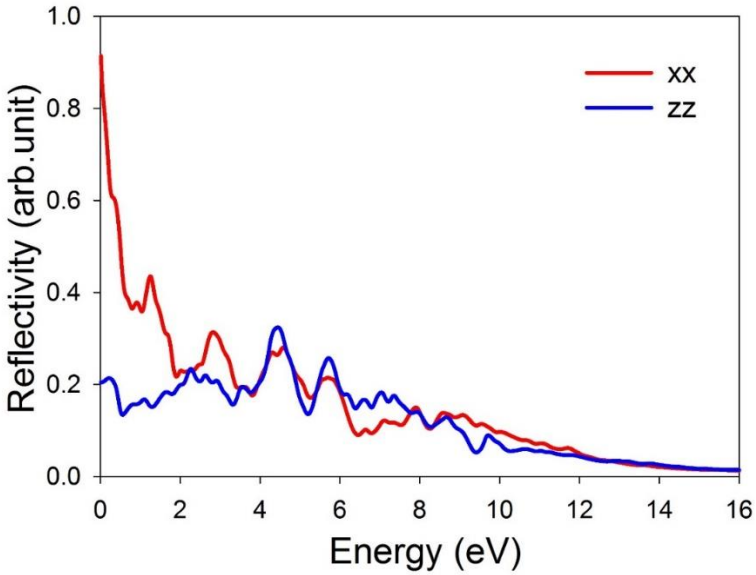


**Fig. 7.** Reflection coefficient for x and z directions in VFeSb structure.

## 4. Conclusion

In general, we proposed the two-dimensional structure of VFeSb by the first principles calculation, then we studied its structural, electronic and optical properties using the density functional theory. The DOS diagram and band structure showed that this structure is conductive in spin up and semi-conductive in spin down, and the whole 2D VFeSb has half-metallic properties and has the correct magnetic moment5 $\mu_B$, while it is a magnetic metal in the bulk state. The biggest effect on changing the electronic properties of VFeSb is related to the d orbitals of two V and Fe atoms. In terms of optical properties, real and imaginary dielectric function curves, energy dissipation function, real and imaginary refractive index and reflection coefficient were investigated for the two symmetrical directions x and z. With a 90 degree change in the direction of the light emitted at low energies, especially in the IR and visible light regions, the 2D structure of VFeSb had an anisotropy property, so it is suitable for an optical switch. Of course, at energies higher than 6 eV, the change in the polarization direction of the structure has isotropic properties. The Re-ε(ω) diagram shows that along the x-axis the behavior of this object is completely metallic and along the z-axis it has a semi-conductive behavior. The maximum electron transition from full to empty levels was observed in the IR and visible light regions. The highest energy loss is in the range of 8-12 eV, but the highest reflection coefficient is in the IR and visible light regions, although the material as a whole has a low reflection coefficient and has a transparent quality.

## References

[1] K. Ono, J. Okabayashi, M. Mizuguchi, Magnetic and electrical properties of zincblende CrAs, et al; J. Appl. Phys. 91, 8088 (2002).

[2] H. Akinaga, T. Manago, M. Shirai, Material Design of Half-Metallic Zinc-Blende CrAs and the Synthesis by Molecular-Beam Epitaxy, Jpn. J. Appl. Phys. Part2 39, L1118 (2000).

[3] M. Mizuguchi, H. Akinaga, T. Manago, et al; Epitaxial growth of zinc-blende CrAs/GaAs multilayer, J. Appl. Phys, 91, 7917 (2002).

[4] R. dePaiva, J.L.A. Alves, R.A. Nogueira, J.R. Leite, L.M.R. Scolfaro, Cubic binary compounds MnN and MnAs and diluted magnetic Ga1-xMnxN semiconductor alloys: a first-principle study, Journal of Magnetism and Magnetic Materials, 288, 384-396 (2005).

[5] R. A. de Groot, F. M. Muller, P. G. van Engen, K. H. J. Buschow, Phys. Rev. Lett; New Class of Materials: Half-Metallic Ferromagnets, 50, 2024 (1983).

[6] I. Galanakis, S. Ostanin, M. Alouani, H. Dreysse, J. M. Will; Phys. Rev. B. 61, 4093 (2000).

[7] X. P. Wei, X. R. Hu, B. Liu, Y. Lei, H. Deng, M. K. Yang, J. B. Deng; Journal of Magnetism and Magnetic Materials, 323, 1606 (2011).

[8] D. P. Rai, R. H. Thapa, Structural, elastic, electronic and magnetic properties of quaternary Heusler alloy Cu2MnSi1-xAlx (x = 0 - 1): First-principles study, Journal of Magnetism and Magnetic Materials; 612, 355 (2014).

[9] A. Birsan, Electronic structure and magnetism of new scandium-based full Heusler compounds: Sc2CoZ (Z=Si, Ge, Sn, Journal of Magnetism and Magnetic Materials; 598, 230 (2014).

[10] N. S. Chauhan, Y. Miyazaki, Low lattice thermal conductivity and microstructural evolution in VFeSb half-Heusler alloys, Materialia, 22, 101430 (2022).

[11] R. Wang, J. Cai, Q. Zhang, X. Tan, J. Wu, G. Liu and J. Jiang, Strong electron–phonon coupling and high lattice thermal conductivity in half-Heusler thermoelectric materials Phys. Chem. Chem. Phys., 26, 8932-8937 (2024).

[12] H. Zhu, W. Li, A. Nozariasbmarz, N. Liu, Y. Zhang, S. Priya, B. Poudel, H-Heusler, alloys as emerging high power density thermoelectric

[13] A. Ojha, R.K. Sabat, S. Bathula, Advancement in half-Heusler thermoelectric materials and strategies to enhance the thermoelectric performance, Materials Science in Semiconductor Processing, 171, 107996 (2024).

[14] Z. Cui, H. Ding, K. Xu, Y. Feng, Electronic structures of various (001) and (111) surfaces, interfaces and spin transport properties of half-metallic fully compensated ferrimagnet Cr2Se, Journal of Alloys and Compounds, 884, 161089 (2021).

[15] H. Han, T. Feng, L. Fan, Z. Zhao, M. Li, K.L. Yao, The half-metallicity of (1 1 1) surface and (1 1 1) interface for Heusler alloy Co2MnGe thin film, Journal of Magnetism and Magnetic Materials, 438, 95-99 (2017).

[16] K. Kasahara, K. Yamamoto, S. Yamada, T. Murakami, K. Hamaya, K. Mibu, M. Miyao, Highly ordered Co2FeSi Heusler alloys grown on Ge(111) by low-temperature molecular beam epitaxy, J. Appl. Phys. 107, 09B105 (2010).

[17] K. Yamada, et.al, Epitaxial growth of a full-Heusler alloy Co2FeSi on silicon by low-temperature molecular beam epitaxy, Thin Solid Films, 518, S278-S280 (2010).

[18] P. Bach, C. Rüster, C. Gould, C. Becker, G.Schmidt, L. W. Molenkamp, Growth of the half-Heusler alloy NiMnSb on (In,Ga)As/InP by molecular beam epitaxy, Journal of Crystal Growth, 251, 323-326 (2003).

[19] E. H. Shourov, R. Jacobs, W. A. Behn, Z. J. Krebs, C. Zhang, P.J. Strohbeen, D. Du, P. M. Voyles, V. W. Brar, D. D. Morgan, and J. K. Kawasaki, Semi-adsorption-controlled growth window for half-Heusler FeVSb epitaxial films, Phys. Rev. Materials 4, 073401 (2020).

[20] A. Boochani, B Nourozi, J. Khodadadi, S. Solaymani, and S. Jalali-Asadabadi, Novel Graphene-like Co2VAl (111): Case Study on Magnetoelectronic and Optical Properties by First-Principles Calculations, J. Phys. Chem., 121, 3978−3986 (2017).

[21] K Schwarz, P Blaha, Computational Materials Science, 28 (2), 259 (2003).

[22] J. P. Perdew, J. A. Chevary, S. H. Vosko, K. A. Jackson, M. R. Pederson, D. Singh and C. Fiolhais, Phys. Rev. B 46, 6671 (1992).

[23] J. P. Perdew, K. Burke and M. Ernzerhof, Phys. Rev. Lett 77, 3865 (1996).

[24] P. Blaha, et. al, An Augmented Plane Wave + Local Orbitals Program for Calculating Crystal Proper-ties, Karlheinz Schwarz, Techn; Universitaetwien: Wein, Austria, 2001.

[25] J. Perdew, Atoms, molecules, solids, and surfaces: Applications of the generalized gradient approximation for exchange and correlation. Phys. Rev. B: Condens. Matter Mater. Phys. 1992, 46, 6671.

[26] R. L. Kronig, J. Opt. Soc. Am. 12 (1926) 547.

[27] M.L. Cohen and J.R.Chelikowsky, Electronic structure and optical properties of semiconductors, second edition, Springer-Verlag Berlin, (1989).

[28] H. Ehrenreich, M.L. Cohen, Self-Consistent Field Approach to the Many-Electron Problem, Phys. Rev. 115 786 (1959).